12-3-2013

Electron-impact vibrational excitation of vibrationally excited H2 molecules [OBJ]involving the resonant 2(Sigma)g+ Rydberg-excited electronic state

R Celiberto
Istituto di Metodologie Inorganiche e Plasmi, CNR, Bari, Italy

R. K. Janev
Macedonian Academy of Sciences and Arts, Skopje, Macedonia

V Laporta
University College London

J Tennyson
University College London

J. M. Wadehra
Wayne State University, ad5541@wayne.edu

Electron-impact vibrational excitation of vibrationally excited H_2 molecules involving the resonant $^2\Sigma_g^+$ Rydberg-excited electronic state

R. Celiberto,[1,2,*] R. K. Janev,[3,4,†] V. Laporta,[5,2,‡] J. Tennyson,[5,§] and J. M. Wadehra[6,‖]

[1]*Dipartimento di Ingegneria Civile, Ambientale, del Territorio, Edile e di Chimica, Politecnico di Bari, Bari, Italy*

[2]*Istituto di Metodologie Inorganiche e Plasmi, CNR, 70125 Bari, Italy*

[3]*Macedonian Academy of Sciences and Arts, Skopje, Macedonia*

[4]*Institute of Energy and Climate Research - Plasma Physics, Forschungszentrum Jülich GmbH Association EURATOM-FZJ, Partner in Trilateral Euregio Cluster, 52425 Jülich, Germany*

[5]*Department of Physics and Astronomy, University College London, London WC1E 6BT, UK*

[6]*Physics Department, Wayne State University, Detroit, Michigan 48202, USA*

(Received 16 August 2013; published 3 December 2013)

Electron-impact theoretical cross sections and rate coefficients for vibrational excitation of vibrationally excited H_2 molecules, occurring through the H_2^- resonant species in the $^2\Sigma_g^+$ Rydberg-excited electronic state, are presented. The cross sections are calculated as functions of the incident electron energy by adopting the local-complex-potential model for resonant collisions and by using *ab initio* calculated molecular potentials and resonance widths. The calculations have been extended to all possible vibrational transitions linking all 15 vibrational levels of the electronic ground state of the H_2 molecule. The corresponding rate coefficients are also obtained as a function of the electron temperature by assuming a Maxwellian electron energy distribution function, and a simple analytical expression is derived. Finally, the present rate coefficients for the transitions starting from the lowest vibrational level of the H_2 molecule are compared with those for the process involving the $X^2\Sigma_u^+$ resonant state of the H_2^- molecular ion.

DOI: 10.1103/PhysRevA.88.062701 PACS number(s): 34.80.Gs, 52.20.Fs

I. INTRODUCTION

Resonant processes involving vibrationally excited H_2 molecules play a role of fundamental importance in affecting the properties of low-temperature hydrogen plasmas, typical of many technological systems. Well-known examples of cold plasmas with a large density of H_2 molecules can be found in nuclear fusion research. This is the case, for instance, of the negative ion sources, designed for the generation and extraction of intense energetic H^- ion beams for heating of plasmas in magnetic fusion devices [1,2]. A second example is provided by the periphery of magnetically confined plasma in toroidal fusion devices, in particular in tokamak divertors, where the relatively low temperatures, dominant in these plasma regions, allow the formation of vibrationally excited diatomic molecules [3,4].

In negative ion sources the production of H^- ions may take place through the well-known dissociative electron attachment (DEA) process, $H_2(v) + e \rightarrow H_2^- \rightarrow H + H^-$, where v is the vibrational quantum number. This reaction involves the resonant molecular state H_2^- and the vibrationally excited ($v \geqslant 0$) neutral molecules. It is well established [1] that this is one of the most relevant processes leading to the formation of negative ions, and its efficiency is strongly enhanced if the molecules are initially in highly excited vibrational levels. These excited molecules, in their turn, are also efficiently formed through the competitive electron-impact-induced resonant vibrational excitation (RVE) process, $H_2(v) + e \rightarrow H_2^- \rightarrow H_2(v') + e$, where the resonant states H_2^- undergo autodetachment with the subsequent formation of possible vibrationally excited $H_2(v')$ molecules. The DEA and RVE processes play an important role also in the volume recombination of divertor plasma. The recombination of the negative ions, formed through the DEA processes sketched above, with the positive H^+ ions leads to the formation of neutral atoms (molecular assisted recombination) which, escaping the guiding magnetic field lines, reduce the localized thermal load on divertor plates [4].

Cross sections for these resonant processes, involving the ground electronic state of the H_2^- transient species, have been calculated and measured over decades, and large sets of data are now available for the applications [5–10]. More recently, the calculations have been extended to the DEA and RVE processes occurring through a Rydberg-excited resonant state of $^2\Sigma_g^+$ symmetry, which is known to give rise to the so-called 14 eV resonance peak in dissociative attachment cross sections [8,11,12] and is also considered responsible for the structures with multiple peaks in the vibrational-excitation cross sections observed in electron-molecule collision experiments [13,14].

A complete set of theoretical vibrational-excitation cross sections and corresponding rate coefficients for dissociative attachment has been obtained, as a function of the electron energy and temperature, respectively, employing the local complex-potential (LCP) formulation of the collision process [15–18] and by using as input parameters of the model, the *ab initio* calculated potential curve and widths of the resonant $^2\Sigma_g^+$ Rydberg state [19]. On the other hand, the cross sections for the RVE process are presently limited to the H_2 excitation starting from the $v = 0$ vibrational level only. In this paper we extend the RVE cross sections, and corresponding rate coefficients, to the whole manifold of the vibrational levels,

*r.celiberto@poliba.it
†r.janev@fz-juelich.de
‡v.laporta@ucl.ac.uk
§j.tennyson@ucl.ac.uk
‖wadehra@.wayne.edu

according to the process

$$\mathrm{H}_2(X\,^1\Sigma_g^+,v) + e(\epsilon_i) \rightarrow \mathrm{H}_2^-(^2\Sigma_g^+)^* \rightarrow \mathrm{H}_2(X\,^1\Sigma_g^+,v') + e(\epsilon_f)\,, \quad (1)$$

where $\mathrm{H}_2^-(^2\Sigma_g^+)^*$ denotes the Rydberg-excited resonant state and the values of the vibrational quantum numbers v,v' range over the interval 0–14. ϵ_i and ϵ_f are the initial and final kinetic energy of the free electron, respectively. The cross-section calculations have been performed in the framework of the LCP model with the same input parameters as employed in Ref. [15], where the differential cross sections for the case $v = 0$ were calculated.

The paper is organized as follows: In Sec. II we give a brief account of the LCP model for resonant collisions, while in Secs. III A and III B the calculated cross sections and rate coefficients, respectively, are presented and discussed. In Sec. IV a short summary of the work is given.

II. THEORETICAL MODEL

In this section only a very brief description is given of the relevant equations of the theoretical model for resonant electron-molecule collisions. A more complete account can be found in previous papers [15,20].

The *local* integral cross-section expression for a resonant excitation, from the vibrational level v to the level v' and for a fixed rotational state $J = 0$, can be written for process (1) as

$$\sigma_{v,v'}(\epsilon_i) = \frac{2\pi^2}{k_i^2}\left|\int_0^\infty dR\,\chi_{v'}^*(R)\Gamma_X^{1/2}(R)\xi_v(R)\right|^2 . \quad (2)$$

k_i is the incident electron's momentum, defined in terms of its kinetic energy ϵ_i as $k_i^2 = 2m\epsilon_i/\hbar^2$, where m is the electron mass. $\chi_{v'}(R)$ is the final vibrational wave function of the target molecule in its ground electronic state, depending on the internuclear distance R. $\Gamma_X(R)$ is the partial width associated with the capture or emission of the free electron from the $X^1\Sigma_g^+$ ground state of the target molecule.

The resonant radial wave function $\xi_v(R)$ is defined by the *local* equation for the nuclear motion,

$$\left[-\frac{\hbar^2}{2M}\frac{d^2}{dR^2} + V^-(R) - \frac{i}{2}\Gamma(R) - E\right]\xi_v(R) = -\left[\frac{\Gamma_X(R)}{2\pi}\right]^{1/2}\chi_v(R). \quad (3)$$

Here M is the nuclei reduced mass, $\chi_v(R)$ is the vibrational wave function in the initial vibrational level v, $\Gamma(R)$ is the total width, and E is the total energy defined by $E = \epsilon_i + E_v$, where E_v is the vth vibrational eigenvalue of the molecule in its ground state. $V^-(R)$ is the potential energy for the Rydberg electronic state $^2\Sigma_g^+$.

In this work, Eq. (3) has been solved by the Green's function method and by using Numerov's algorithm for the calculation of the regular and irregular wave functions needed to build Green's function (see Appendix). The input parameters $V^-(R)$, $\Gamma(R)$, and $\Gamma_X(R)$ are all taken from the *ab initio* calculations of Ref. [19] and extrapolated to the extreme regions ($R \rightarrow 0,\infty$) according to Ref. [15].

Finally, the rate coefficients for process (1) have been also calculated according to the expression

$$\kappa_{v,v'}(T) = \sqrt{\frac{8}{m\pi}}\left(\frac{1}{T}\right)^{3/2}\int_{\epsilon_{\mathrm{th}}}^\infty d\epsilon_i\,\epsilon_i\,e^{-\frac{\epsilon_i}{T}}\,\sigma_{v,v'}(\epsilon_i), \quad (4)$$

obtained by assuming a Maxwellian electron energy distribution function, at the electron temperature T, in energy units, and where ϵ_{th} represents the threshold energy for the $v \rightarrow v'$ excitation.

III. RESULTS

A. Cross sections

Integral RVE cross sections have been calculated using Eq. (2) for all the excitation processes with $v' \geqslant v$, where v runs from 0 through 14. The cross sections for the deexcitation ($v < v'$) can be obtained via detailed balance [21]. The results obtained are shown in Figs. 1–5 as a function of the incident electron energy. In these figures some curves do not appear since the cross sections are very small. The other visible curves are labeled with the corresponding value of v'.

The left upper panel of Fig. 1 shows the cross sections for the $0 \rightarrow v'$ transitions. For the inelastic process ($v' \neq 0$), the corresponding differential cross sections, at an angle of 85°, have been calculated in Ref. [15] by using the same method and input parameters adopted in the present paper and were found to be in good agreement with the measurements reported in Ref. [13].

We have also extended the sensitivity analysis, performed in Ref. [15] for the $v = 0$ cross sections, to the levels $v,v' = 5$, 10, and 14, by altering separately the input parameters [$\Gamma(R)$,$\Gamma_X(R)$, and $V^-(R)$] by ±10% and observing the cross-section variations. We explored the energy regions for the above transitions where the cross sections are appreciably different from zero characterized, in particular, by the appearance of sharp peaks. Outside these regions the cross sections become vanishingly small and the numerical accuracy in the calculations accordingly tends to decrease.

An alteration of ±10% in $\Gamma(R)$ does not affect the cross section for the transition $5 \rightarrow 5$ in the region of 10–12 eV, while for the cases $5 \rightarrow 10$ and $5 \rightarrow 14$, the cross-section variation is no larger than 10%. In general, the cross-section variation is quite contained at the peaks, due to their large values, and decreases between the peaks and in the far energy regions, where the cross sections are characterized by small values. This is particularly true for the elastic processes which show the largest cross sections. For the transition $10 \rightarrow 10$, for example, the variation of $\Gamma(R)$ induces a change in the cross section of about 0.05% at the main peak ($\sigma = 9 \times 10^{-19}$ cm^2, see Fig. 4), which rises to 0.3% at the minimum placed at 9.18 eV ($\sigma = 4 \times 10^{-20}$ cm^2), then becomes ∼3% at 10.02 eV, where the cross section starts to vanish ($\sigma = 6 \times 10^{-21}$ cm^2). For the inelastic transition $10 \rightarrow 14$, the cross sections are generally smaller than the previous cases, so reduced accuracy is to be expected. In fact, at the main peak, the accuracy is about 6% and reaches ∼20% at 9.68 eV between two peaks ($\sigma = 8 \times 10^{-23}$ cm^2). The same

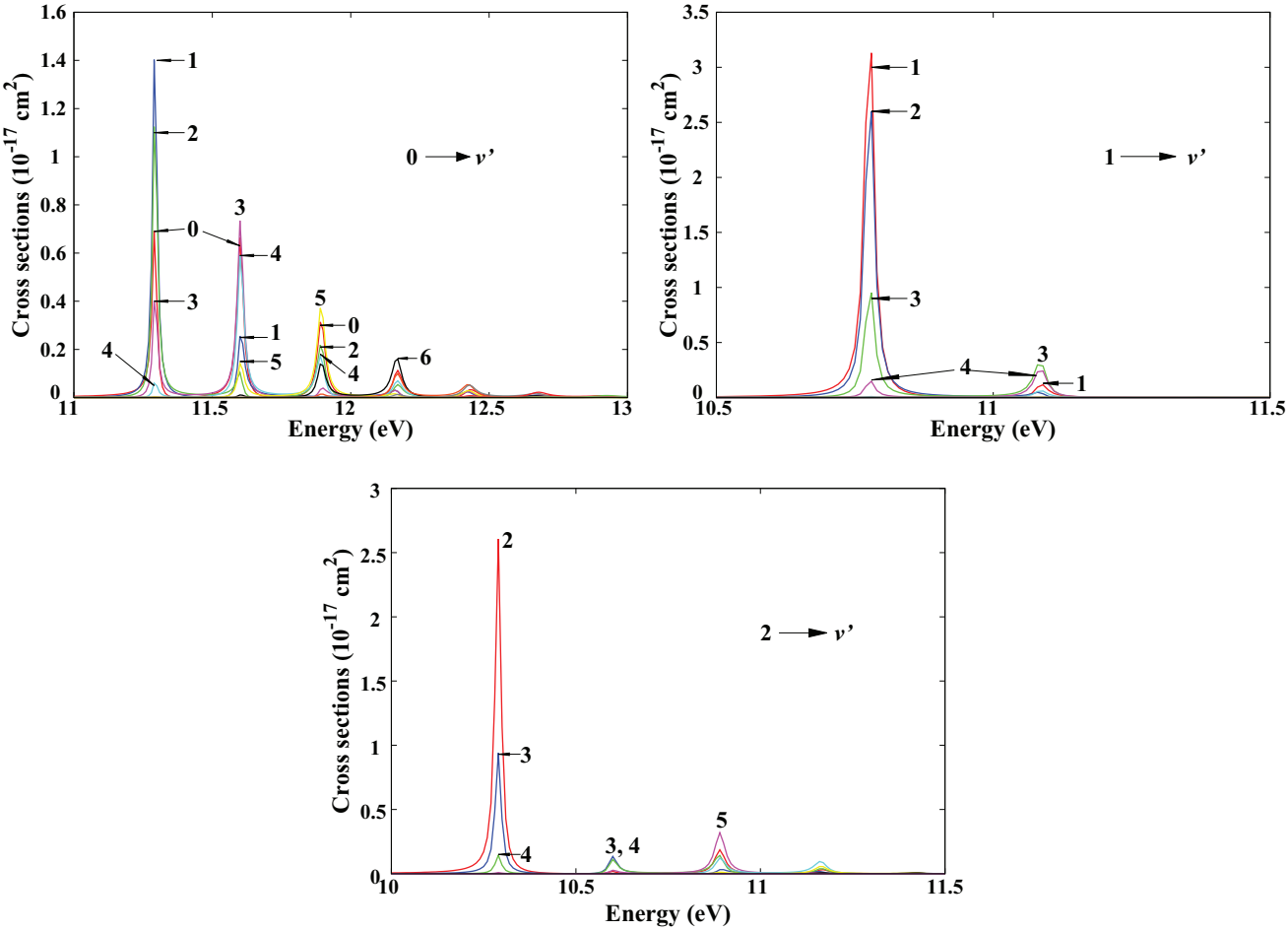

FIG. 1. (Color online) Resonant excitation cross sections as a function of the incident electron energy for the transition $v \to v'$ where $v = 0,1,2$, as indicated in the three panels, respectively, and $v' \geqslant v$. Each visible curve in the figures is labeled with the corresponding value of v' (see text).

situation is observed for the $14 \to 14$ transition, where the largest variation does not exceed 15%.

The influence of an alteration of $\pm 10\%$ of $\Gamma_X(R)$ on the cross sections is not substantially different from the previous case. For the transitions $5 \to 5,10,14$ the largest cross-section variation is smaller than 10%, being almost zero for the elastic process. For the $10 \to 10,14$ excitations the variations are less than 1% and 20% for the elastic and inelastic processes, respectively. Finally, for the $14 \to 14$ transition, the variation remains confined within 15%.

A modification of $\pm 10\%$ of the potential $V^-(R)$ does not produce significant variation in the cross section for the elastic transition $5 \to 5$, where the largest discrepancy between peaks is less than 2%. For the $5 \to 10$ case, the variation in the 10–11 eV energy interval is <4% and grows for $\epsilon_i > 11$ eV, where the cross sections start to decrease. For the $5 \to 14$ the variation in the peak region is not larger than 20%. For the $10 \to 10$ case, the cross section variation in the interval 8.5–9.5 eV is contained within 5% and reaches 20% in the interval 9–10 eV for the $10 \to 14$ transition. Finally, for the $14 \to 14$ process, the variation in the largest cross section is up to 10%.

The sharp and thin peaks observed in the figures indicate that the resonant process is characterized by small widths. This implies a long lifetime for the resonant $H_2^-(^2\Sigma_g^+)$ Rydberg state, which thus behaves like a quasi-stable molecular ion. The peak positions of the cross sections, in fact, fall almost exactly at the vibrational eigenvalues of the resonant states, and the small energy spread determines a narrow profile of the cross-section curves.

This can be better seen in Figs. 6(a) and 6(b) where the cross sections for the $0 \to 0$ and $5 \to 5$ elastic transitions are shown in logarithmic scale. The structures in these two figures are typical boomerang oscillations, which have been observed since early calculations and experiments on the RVE process in H_2 [10,23]. The crosses, over the lower and upper energy axis, locate the energy of the resonant vibrational eigenvalues [22] E_{v_r} above the target levels, i.e., the difference $\Delta E_{v_r} = E_{v_r} - E_v$, for $v = 0$ and 5 respectively. The vertical lines, connecting the crosses, coincide with the energy positions of the cross section peaks, showing clearly their correspondence with the resonant vibrational energies [24]. This however is not always true. In some cases, in fact, we have found that expected peaks are missing. Figure 6(b) provides an example. At the energy corresponding to $E_{v_r=6} - E_{v=5} = 10.61$ eV (7-th line in the figure), in fact, no peak is observed.

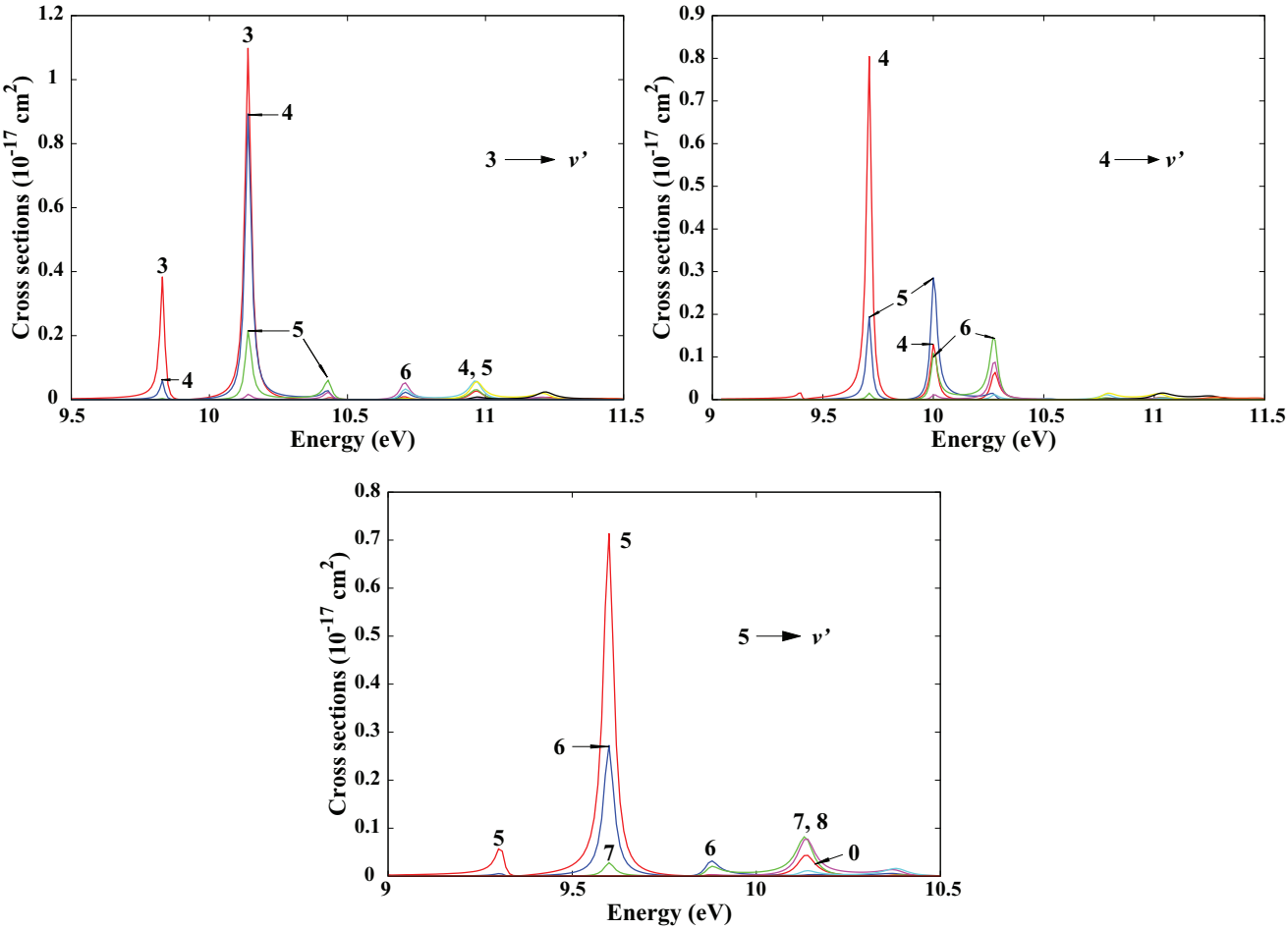

FIG. 2. (Color online) Same as Fig. 1, but for $v = 3,4,5$.

This can be explained by writing the resonant nuclear wave function as (see Appendix)

$$\xi_v(R) = -\int_0^\infty dR' \left[\sum_{v_r} C_{v_r}(R')\varphi_{v_r}(R)\right]\left[\frac{\Gamma_X(R')}{2\pi}\right]^{1/2}\chi_v(R'), \tag{5}$$

where the quantity in the first bracket is the resonant Green's function expressed as a linear combination of the vibrational wave functions of the resonant state, $\varphi_{v_r}(R)$. Inserting now Eq. (5) in Eq. (2) and assuming that the width, in the spirit of the Frank-Condon principle, can be approximated as $\Gamma_X(R) = \Gamma_X(R') \approx \Gamma_X(\bar{R})$, where $\bar{R}$ is a suitable value of the internuclear distance such that $\Gamma_X(\bar{R})$ can be carried out of the integral, and putting, according to Eq. (A9), $C_{v_r}(R') \approx 2i\varphi^*_{\bar{v}_r}(R')/\Gamma_{\bar{v}_r\bar{v}_r}$, we can write finally for $v = v'$,

$$\sigma_{v,v}(\epsilon_i) \approx \frac{4\pi}{k_i^2}\,\Gamma_X^2(\bar{R})\left|\frac{Q_{\bar{v}_r,v}\,Q_{v,\bar{v}_r}}{\Gamma_{\bar{v}_r,\bar{v}_r}}\right|^2 = \frac{4\pi}{k_i^2}\,\Gamma_X^2(\bar{R})\frac{|Q_{\bar{v}_r,v}|^4}{|\Gamma_{\bar{v}_r,\bar{v}_r}|^2}, \tag{6}$$

where $Q_{\bar{v}_r,v} = \int dR\varphi^*_{\bar{v}_r}(R)\chi_v(R) = Q^*_{v,\bar{v}_r}$. Equation (6) shows that the cross section is mainly governed by the *resonant* Franck-Condon factors $Q_{\bar{v}_r,v}$, while the matrix elements $\Gamma_{\bar{v}_r,\bar{v}_r}$ are found to be quite insensitive to the variations of the quantum number $\bar{v}_r$. This can be seen in Table I, which reports the calculated values of both $|\Gamma_{\bar{v}_r,\bar{v}_r}|^2$ and $|Q_{\bar{v}_r,v=5}|^4$. The table also shows that for $v_r = 5$ and 7, $|Q_{\bar{v}_r,5}|^4$ is very large, compared with the case $\bar{v}_r = 6$, and this explains the formation of the peaks, in Fig. 6(b), in correspondence with the energy of these two levels of 10.38 and 10.87 eV, respectively. $|Q_{\bar{v}_r,5}|^4$ for $v_r = 6$ is instead three orders of magnitude smaller than the other two cases, and this explains the missed peak in the cross sections at the expected energy of $E_{v_r=6} - E_{v=5} = 10.61$ eV. The consequence, from a physical point of view, is that the formation of the resonant state, when the incident electron energy is close to 10.61 eV and the target molecule is initially in the excited level $v = 5$, is counteracted by the nuclear motion which has a small probability of transiting from the energy level $v = 5$ to the resonant level $v_r = 6$, due to the unfavorable interference of the corresponding vibrational wave functions.

Another interesting aspect is represented by the fact that the sharp cross-section peaks end at the energy of the last resonant vibrational level, in the region where the resonant continuum starts. Beyond this point, wide oscillations appear in high-energy cross-section tail [see Fig. 6(b)]. These structures are present also for other transitions, elastic or inelastic, and even for different molecules [25,26].

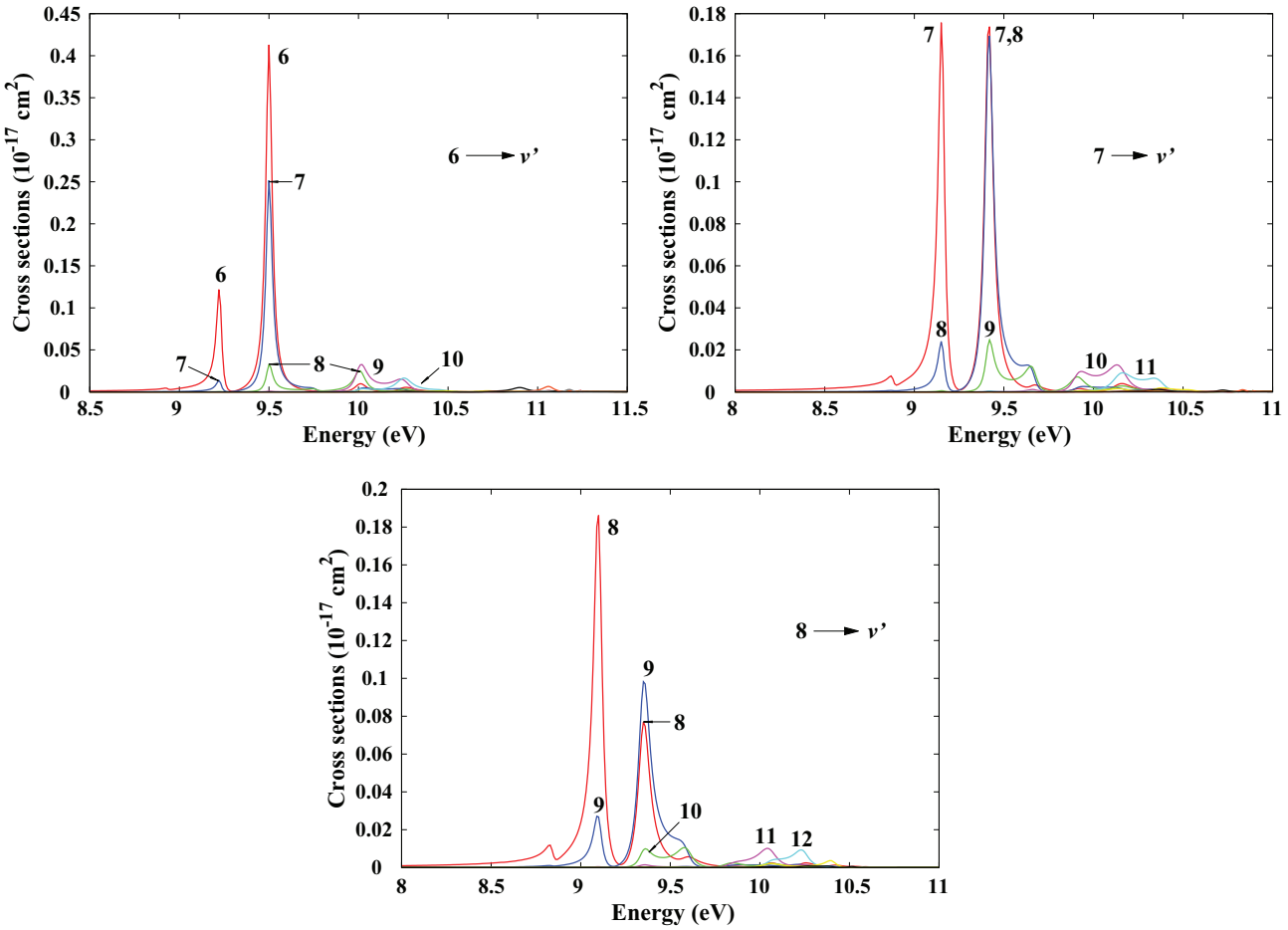

FIG. 3. (Color online) Same as Fig. 1, but for $v = 6,7,8$.

A clear example can be seen in Fig. 7, where the cross sections for the elastic transition $10 \rightarrow 10$ (full-blue line) are shown. Once again, the neutral-resonant vibrational overlap governs this behavior. To show this effect, we can rewrite the cross section again in terms of Green's function, namely (see Appendix),

$$\sigma_{v,v'}(\epsilon_i) = \frac{2\pi^2}{k_i^2}\left|\int_0^\infty\int_0^\infty dR\,dR'\chi^*_{v'}(R)\Gamma_X^{1/2}(R) \times\left(\sum_{v_r}\!\!\!\!\!\!\int C_{v_r}(R')\varphi_{v_r}(R)\right)\left[\frac{\Gamma_X(R')}{2\pi}\right]^{1/2}\chi_v(R')\right|^2. \tag{7}$$

The quantity in parentheses can now be written explicitly in terms of the two contributions as $\sum\!\!\!\!\!\!\int_{v_r} = \sum_{\text{b.s.}} + \int_c$, where the sum on the r.h.s is extended to the bound vibrational states and the integration to the continuum. In this way we may include or exclude the continuum in Eq. (7) at will. We have recalculated the cross sections for the $10 \rightarrow 10$ transition using Eq. (7) without the continuum and the result is shown in Fig. 7 (dot-red line) along with the cross sections obtained assuming a Green's function of the form (A3) (full-blue line). This figure provides evidence of the role of the resonant vibrational continuum on the cross-section oscillations for high energies. Similar oscillations were already observed in the corresponding dissociative attachment process, involving the same Rydberg state [17]. This process in fact, also occurs when the total scattering energy is above the dissociation limit of the resonant state, and the DEA oscillating behavior was demonstrated to be determined by the vibrational overlap of the Rydberg continuum and H_2 bound wave functions [17].

B. Rate coefficients

The rate coefficients, for the transitions $v \rightarrow v'$ of process (1), calculated by Eq. (4) in the range of the electron temperature of 0.1–1000 eV (see Sec. IV), are shown for some cases in Fig. 8, where for clarity the range of temperatures was cut to 100 eV. In each panel, all the rate maxima occur practically at the same temperature; and the largest rates, as expected, are those corresponding to the elastic processes. The general behavior is similar for all the curves, the difference being of a quantitative nature only. This regularity suggests that some universal fitting function can be found.

To get such a function we may try for the cross section the following ansatz:

$$\sigma_{v,v'}(\epsilon_i) = \alpha\,\sigma_{v,v'}\left(\Delta E_p^L\right)\,\delta\left(\epsilon_i - \Delta E_p^L\right), \tag{8}$$

where ΔE_p^L is the energy position of the largest cross-section peak, for the given transition $v \rightarrow v'$, $\sigma_{v,v'}(\Delta E_p^L)$ the corresponding peak value, and $\delta(\epsilon_i - \Delta E_p^L)$ is the Dirac δ

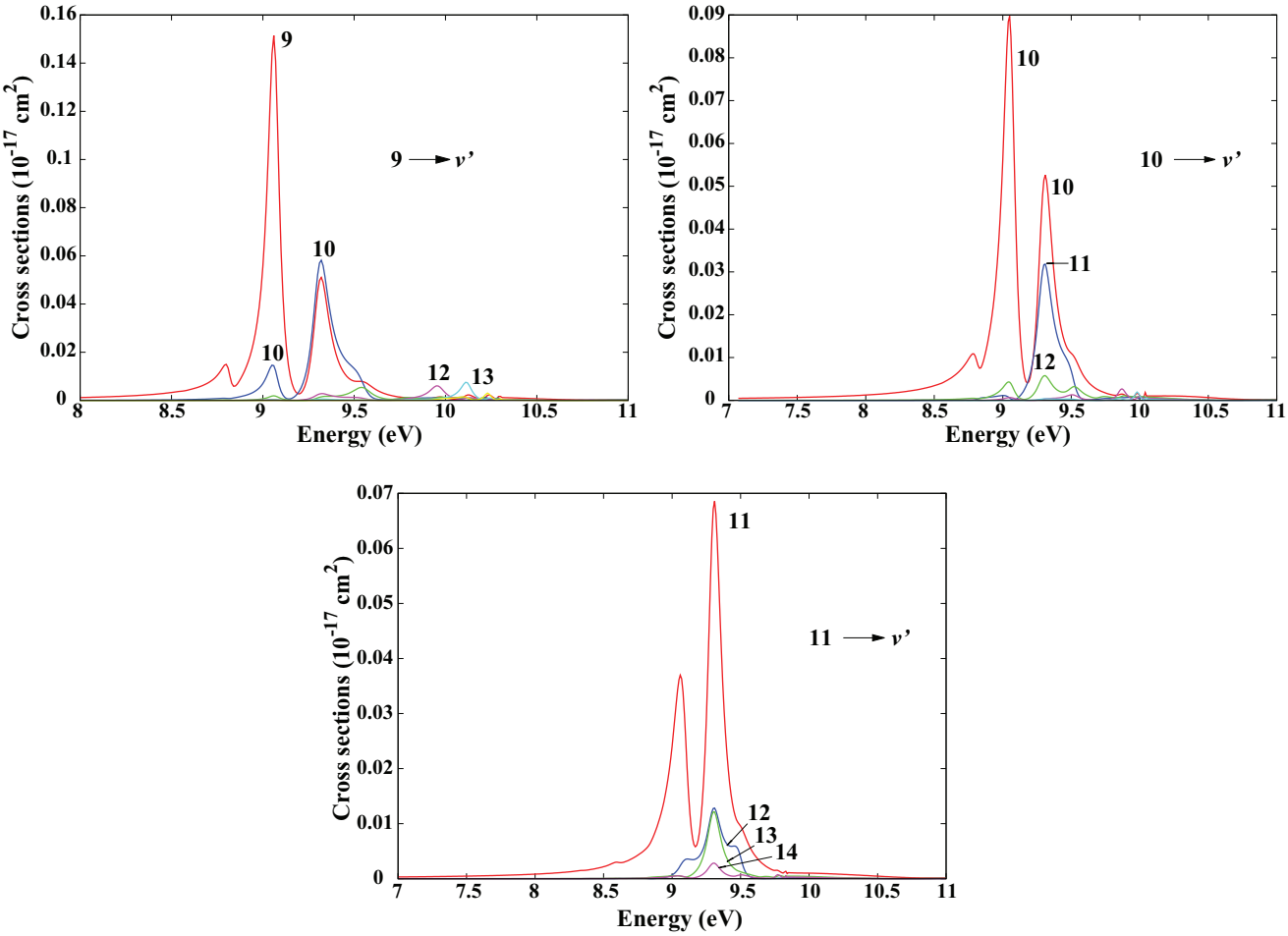

FIG. 4. (Color online) Same as Fig. 1, but for $v = 9,10,11$.

function. α is an unessential constant with the dimension of energy, introduced for dimension consistency. In view of the final normalization, it can be assumed equal to 1 without affecting the treatment. The δ-function behavior is justified by the sharp nature of the peaks, all placed, as we have seen, at energies ΔE_p, and by the fact that in general only one peak, of very large intensity, dominates over the others. Substituting Eq. (8) in Eq. (4), the integral is immediate, so one gets

$$\kappa_{v,v'}(T) \approx \sqrt{\frac{8}{m\pi}}\,\sigma_{v,v'}\left(\Delta E_p^L\right)\left(\frac{1}{T}\right)^{3/2}\Delta E_p^L\, e^{-\frac{\Delta E_p^L}{T}}. \quad (9)$$

It can now be easily shown, by constraining the first derivative to vanish, that the maximum of this expression occurs at the temperature $T_{\max} = \frac{2}{3}\Delta E_p^L$, and its value $\kappa_{v,v'}^{\max}$ is given by

$$\kappa_{v,v'}^{\max} = \sqrt{\frac{8}{m\pi}}\,\sigma_{v,v'}\left(\Delta E_p^L\right)\left(\frac{3}{2}\right)^{3/2} e^{-\frac{3}{2}}\left(\Delta E_p^L\right)^{-1/2}$$
$$= 0.409916\,\sqrt{\frac{8}{m\pi}}\,\sigma_{v,v'}\left(\Delta E_p^L\right)\left(\Delta E_p^L\right)^{-1/2}. \quad (10)$$

Inserting this expression in Eq. (9) we obtain

$$\kappa_{v,v'}\left(\Delta E_p^L \tau\right) \approx \kappa_{v,v'}^{\max}\left(\frac{1}{\tau}\right)^{3/2} e^{-\frac{1}{\tau}}, \quad (11)$$

where τ, the reduced temperature, is defined by $\tau = T/\Delta E_p^L$ and $\kappa_{v,v'}^{\max}$ includes also the factor $1/0.409916$. The desired universal function is represented by $\tau^{-3/2}\, e^{-\frac{1}{\tau}}$, which is expected to reproduce the general shape of all the rate coefficients. Once this quantity is multiplied by $\kappa_{v,v'}^{\max}$, Eq. (11) provides the fitting expression for the rate coefficients. $\kappa_{v,v'}^{\max}$ can be taken from the calculated rates, so that Eq. (11) is automatically normalized to these last quantities. Its values are provided in Table II for all the $v \to v'$ ($v' \geqslant v$) transitions. The rate coefficients for the inverse processes ($v' < v$) can be obtained, as already stated, by detailed balance [21], once the transition energies $\Delta E_{v,v'} = E_{v'} - E_v$ are provided [27,28]. Regarding the energy positions of the largest peaks, according to our simple δ-function model, they should depend on both v and v' levels. However, we verified that no appreciable difference can be observed in the fitted rates if we assume

TABLE I. Values of the matrix elements $|\Gamma_{\bar{v}_r,\bar{v}_r}|^2$ and the resonant Franck-Condon factors $|Q_{\bar{v}_r,v}|^4$ for $v = 5$ and $v_r = 5,6,7$ (see text).

v_r	$\lvert\Gamma_{\bar{v}_r,\bar{v}_r}\rvert^2$	$\lvert Q_{\bar{v}_r,5}\rvert^4$
5	8.6×10^{-6}	1.4×10^{-3}
6	1.6×10^{-5}	2.5×10^{-6}
7	2.3×10^{-5}	1.3×10^{-3}

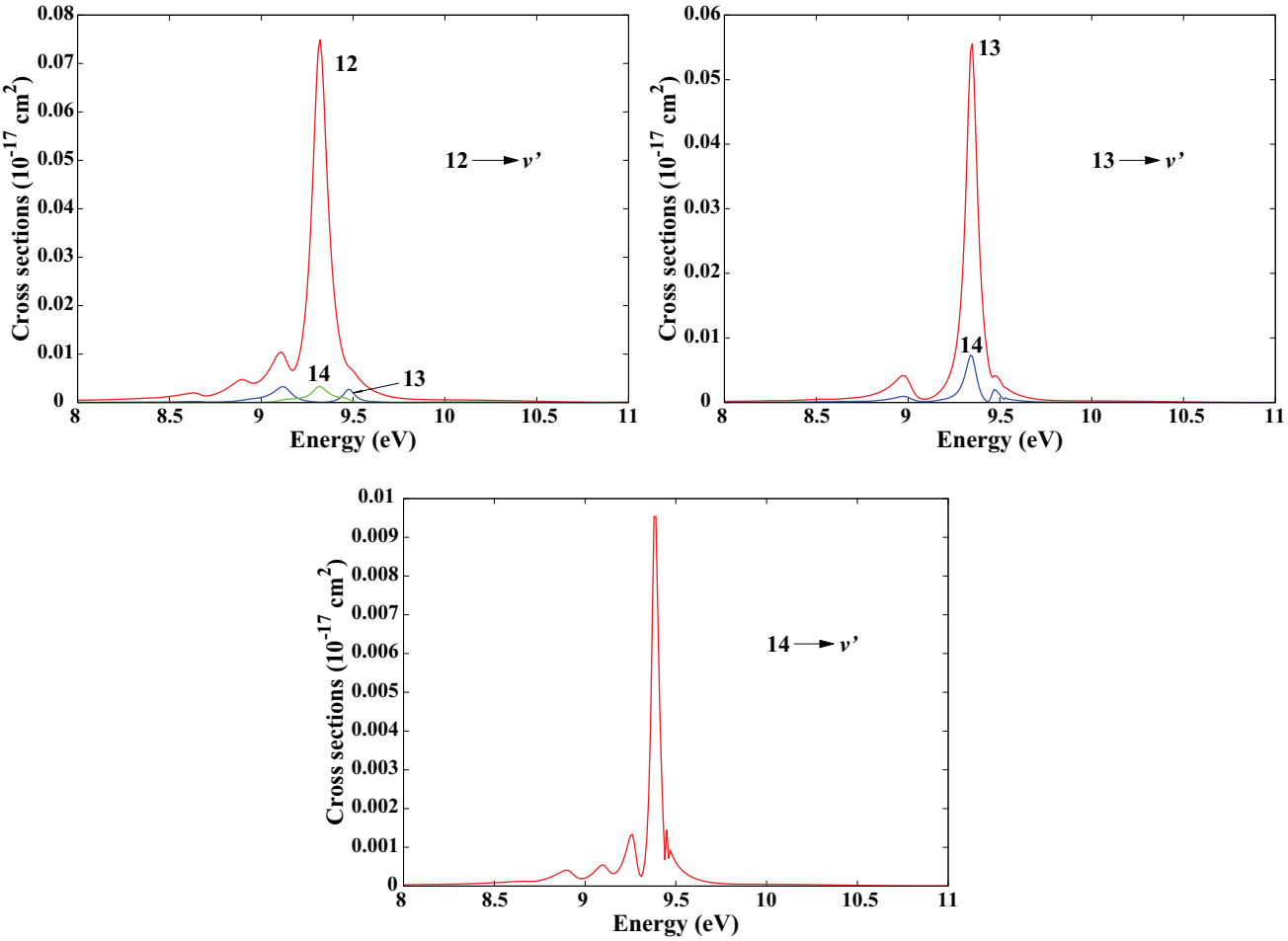

FIG. 5. (Color online) Same as Fig. 1, but for $v = 12, 13, 14$.

for a given v that $\Delta E_p^L(v,v') \approx \Delta E_p^L(v,v)$. This reduces the number of parameters required in Eq. (11). This approximation is justified by the fact, noted above, that all the maxima of the rate coefficients for a given v and different v' fall practically at the same temperature, and this temperature, as we have seen, is linked to the energy positions by the relation $T_{\max} = \frac{2}{3}\Delta E_p^L$, which gives, in addition, a more concrete physical meaning to these parameters. The elastic $\Delta E_p^L(v = v')$ energies are also provided in the last column of Table II. Examples of rate fittings are shown also in Fig. 8. The agreement among the calculated and fitted rate coefficients is exceptionally good.

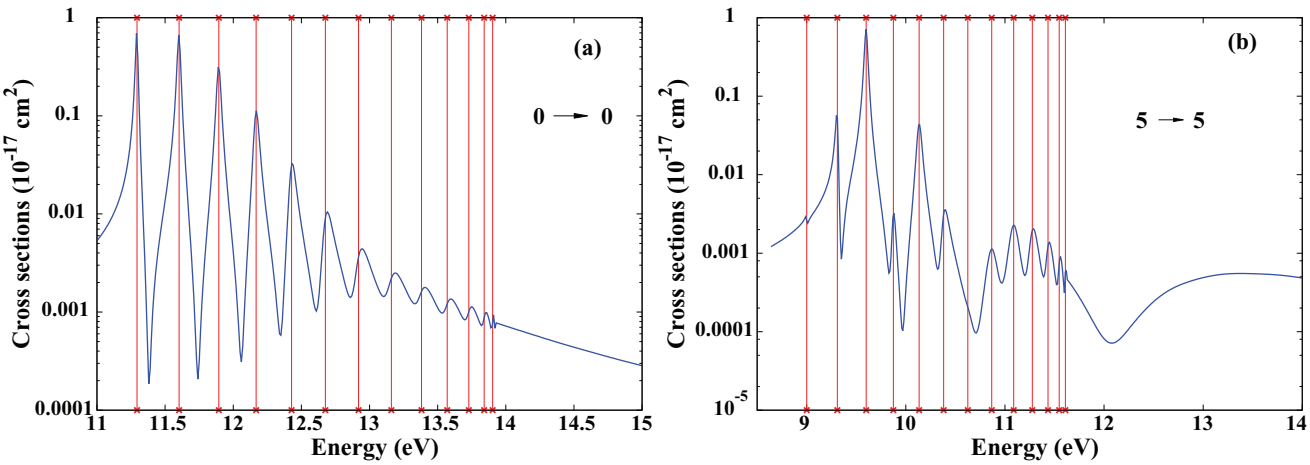

FIG. 6. (Color online) Cross sections for the elastic (a) $0 \rightarrow 0$ and (b) $5 \rightarrow 5$ transitions. The crosses over the lower and upper energy axis, connected by vertical lines, locate the $^2\Sigma_g^+$ resonant state vibrational eigenvalues.

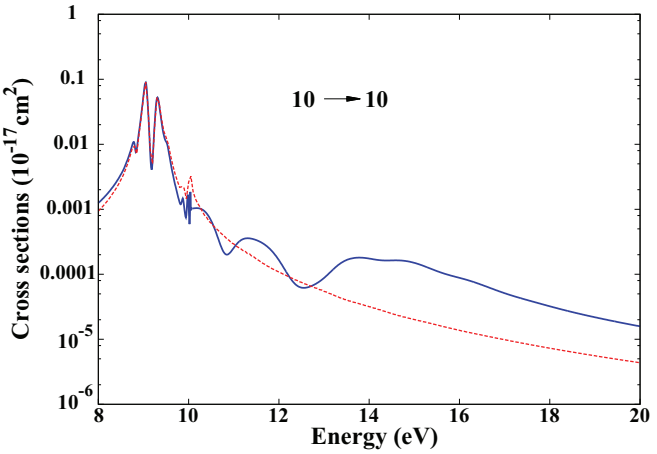

FIG. 7. (Color online) RVE cross sections for the $10 \rightarrow 10$ transition (full-blue curve). The dot-red curve represents the cross sections calculated by Eq. (7) where the contribution from the vibrational continuum was excluded (see text).

To assess the role of the RVE process in hydrogen plasmas, we have compared the present rate coefficients with those for the vibrational excitation occurring through the $X^2\Sigma_u^+$ state of the H_2^- ion, generated after the trapping of the incident electron inside the centrifugal barrier associated with the $l = 1$ partial wave (shape resonance). This resonant state is known to play a role of great importance in hydrogen plasmas [1–4], and cross sections for the RVE process involving the shape resonance have been reported in the literature by many authors [5,7,10]. On the other hand, to the best of our knowledge, theoretical calculations or experimental measurements for rate coefficients are practically nonexistent. So, to perform the above comparison, we have calculated the cross sections for the $0 \rightarrow v'$ RVE transitions occurring through the $X^2\Sigma_u^+$ state by adopting the computational model of Ref. [5]. Then, from Eq. (4), the corresponding rate coefficients were obtained.

Figure 9 shows the rate coefficients for the inelastic transitions $0 \rightarrow v'$ as a function of the final vibrational levels and for RVE processes occurring through both the shape and Rydberg resonances at a fixed temperature of 8 eV, closely corresponding to the maxima of the Rydberg rates. The figure shows that the rate coefficients for the shape resonance decrease rapidly with the final quantum number becoming, for $v' > 4$, smaller than the corresponding values for the Rydberg resonance by several orders of magnitude. Actually, we have observed the same behavior in a wide range of temperatures ($T \sim$ 2–1000 eV) and only for temperatures below ~2 eV do the rates for the Rydberg resonance show a fast decrease and become, at very low temperatures of the investigated range, dramatically smaller than the corresponding rates for the shape resonance. This indicates that in hydrogen plasmas characterized by high temperatures, typical, for example, of edge and divertor regions of the fusion reactors, the RVE process involving the Rydberg resonance could have a prominent role

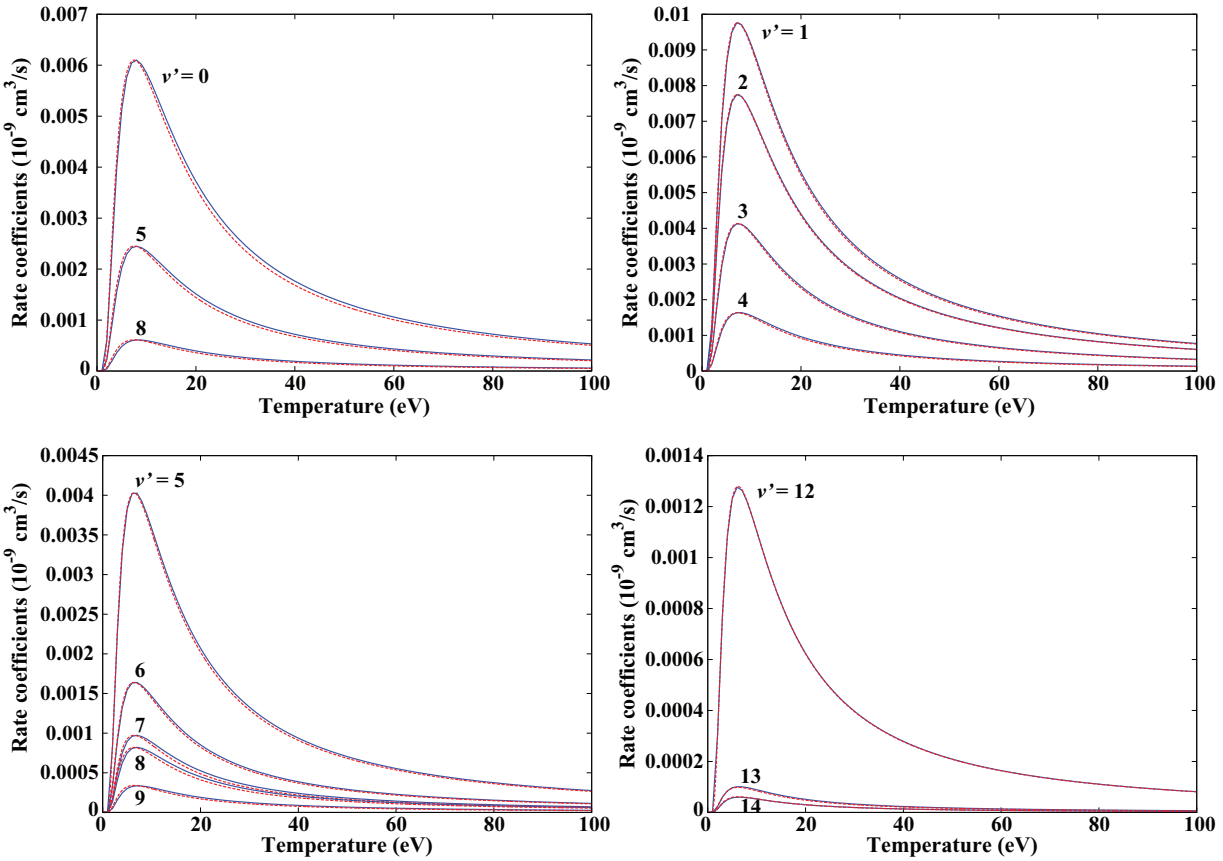

FIG. 8. (Color online) Comparison among the calculated (full-blue curves) and fitted (dot-red) curves for the transitions $v = 0,1,5,12 \rightarrow v'$ where the values of $v' \geqslant v$ are indicated in the panels.

TABLE II. $\kappa_{\max}^{v,v'}$ (10^{-9} cm^3/s), with $v' \geqslant v$, and largest peak position energies ΔE_p^L (eV). The notation such as 1.488(−2) stands for 1.488×10^{-2}.

v' \ v	0	1	2	3	4	5	6
0	1.488(−2)						
1	1.247(−2)	2.381(−2)					
2	1.137(−2)	1.891(−2)	1.952(−2)				
3	1.012(−2)	1.008(−2)	8.10(−3)	1.300(−2)			
4	8.25(−3)	3.98(−3)	4.24(−3)	9.25(−3)	9.98(−3)		
5	5.98(−3)	1.44(−3)	4.17(−3)	3.51(−3)	5.56(−3)	9.83(−3)	
6	3.95(−3)	1.15(−3)	2.88(−3)	1.56(−3)	3.88(−3)	4.00(−3)	7.98(−3)
7	2.46(−3)	1.46(−3)	1.29(−3)	1.76(−3)	1.78(−3)	2.37(−3)	4.20(−3)
8	1.49(−3)	1.59(−3)	5.1(−4)	1.66(−3)	7.3(−4)	2.00(−3)	1.44(−3)
9	8.5(−4)	1.41(−3)	4.1(−4)	9.5(−4)	9.3(−4)	8.3(−4)	1.44(−3)
10	4.4(−4)	1.00(−3)	5.6(−4)	3.2(−4)	8.8(−4)	4.4(−4)	8.1(−4)
11	2.0(−4)	5.9(−4)	5.6(−4)	1.7(−4)	4.1(−4)	5.4(−4)	2.4(−4)
12	1.0(−4)	3.7(−4)	4.4(−4)	2.0(−4)	1.7(−4)	3.9(−4)	2.7(−4)
13	5.(−5)	2.0(−4)	2.7(−4)	1.5(−4)	1.0(−4)	2.2(−4)	2.2(−4)
14	2.(−5)	7.(−5)	1.2(−4)	7.(−5)	2.(−5)	7.(−5)	1.0(−4)

v' \ v	7	8	9	10	11	12	13	14	ΔE_p^L
0									10.780
1									11.290
2									10.290
3									10.140
4									9.711
5									9.600
6									9.500
7	6.44(−3)								9.155
8	4.03(−3)	6.22(−3)							9.100
9	1.20(−3)	3.49(−3)	6.46(−3)						9.064
10	8.8(−4)	8.3(−4)	2.63(−3)	5.95(−3)					9.519
11	6.1(−4)	5.6(−4)	4.6(−4)	1.44(−3)	4.54(−3)				9.304
12	2.2(−4)	4.6(−4)	3.9(−4)	6.1(−4)	7.3(−4)	3.12(−3)			9.317
13	1.2(−4)	2.2(−4)	2.7(−4)	2.0(−4)	5.4(−4)	2.4(−4)	1.61(−3)		9.345
14	5.(−5)	7.(−5)	1.0(−4)	7.(−5)	1.7(−4)	1.5(−4)	2.7(−4)	2.2(−4)	9.381

in contributing to the nonequilibrium overpopulation of the high vibrational levels.

IV. SUMMARY

We have calculated the electron-impact vibrational excitation cross sections for the scattering process involving vibrationally excited H_2 molecules, and occurring through the formation of the H_2^- transient species in the resonant Rydberg-excited electronic state $^2\Sigma_g^+$. The cross sections are calculated, as a function of the incident electron energy, by using the local complex-potential model and for all possible $v \to v'$ vibrational transitions with $v' \geqslant v$. Cross sections for the inverse transition can be obtained by detailed balance. The main feature of the calculated cross sections is the appearance of sharp and narrow peaks located at energies corresponding to vibrational level eigenvalues of the $^2\Sigma_g^+$ electronic state. In some cases, however, expected peaks are absent, suppressed by the small value of the neutral-ion vibrational wave function overlap. A second aspect of the calculated cross section is represented by their oscillations above the dissociation threshold of the Rydberg state, determined by the vibrational wave function overlap of the resonant and target electronic states.

The corresponding rate coefficients for the same vibrational excitations were also calculated as a function of the electron temperature and by assuming a Maxwellian electron distribution function. An accurate fit expression for the calculated rates has been also derived by assuming a simple δ function model for the cross sections. Finally, a comparison of the rate coefficients for the RVE processes $0 \to v'$, involving the $H_2^-(X^2\Sigma_u^+)$ resonant state with the Rydberg rates, shows that for high vibrational levels these last quantities exceed the former by orders of magnitude, which suggests a significant influence on the vibrational kinetics of high-temperatures H_2 plasmas.

The whole cross section and rate coefficient data set presented here, extended to the range of collision energies of 0–20 eV and temperatures of 0.1–1000 eV, respectively, is available online [31].

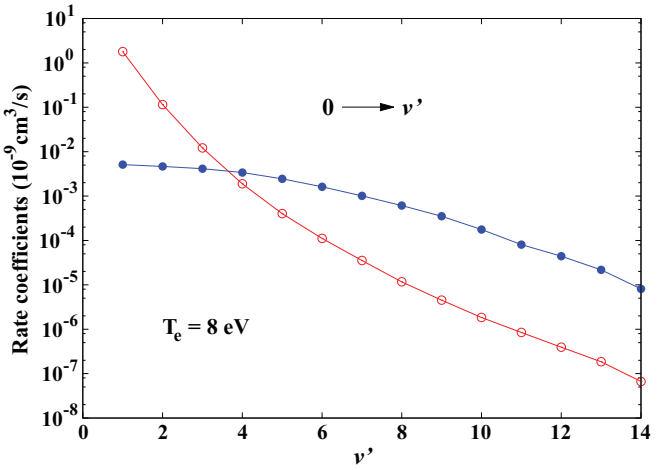

FIG. 9. (Color online) Comparison between the rate coefficients as a function of the final vibrational level $v' \geqslant 1$ and calculated at an electronic temperature of 8 eV for the processes (a) $H_2(X^1\Sigma_g^+, v=0)+e \rightarrow H_2^-(X^2\Sigma_u^+) \rightarrow H_2(X^1\Sigma_g^+, v')$ (red-open circles) and (b) $H_2(X^1\Sigma_g^+, v=0)+e \rightarrow H_2^-(\text{Rydberg}\ ^2\Sigma_g^+) \rightarrow H_2(X^1\Sigma_g^+, v')$ (blue-filled circles).

ACKNOWLEDGMENT

The present work has been financed by the European Community's Seventh Framework Programme (FP7/2007-2013) under Grant Agreement No. 242311.

APPENDIX: GREEN'S FUNCTION CALCULATION

The nuclear resonant wave function can be obtained from Eq. (3) written in integral form as [29]

$$\xi_v(R) = -\int_0^\infty dR'\, G(R,R')\left[\frac{\Gamma_X(R')}{2\pi}\right]^{1/2}\chi_v(R'), \quad \text{(A1)}$$

where Green's function, $G(R,R')$, obeys the equation

$$\left[-\frac{\hbar^2}{2M}\frac{d^2}{dR^2} + V^-(R) - \frac{i}{2}\Gamma(R) - E\right]G(R,R') = \delta(R-R'). \quad \text{(A2)}$$

Green's function can be calculated by following two different standard treatments [30]. The first approach consists in building the function $G(R,R')$ by obtaining two independent solutions of the homogeneous equation associated with Eq. (A2), say $u(R)$ and $v(R)$, which can be used to write Green's function as

$$G(R,R') = -\frac{1}{W}u(R_>)v(R_<), \quad \text{(A3)}$$

where, as usual, $R_>$ and $R_<$ denote the greater and the smaller between R and R', and W gives the Wronskian defined by $W = u'(R)v(R) - u(R)v'(R)$.

A second way to calculate Green's function is represented by the expansion of $G(R,R')$ in terms of an orthonormal set of basis functions, $\varphi(R)$, as [29,30]

$$G(R,R') = \sum_n C_n(R')\varphi_n(R) + \int d\epsilon\, C_\epsilon(R')\varphi_\epsilon(R) = \sum\!\!\!\!\!\!\int_\nu C_\nu(R')\varphi_\nu(R), \quad \text{(A4)}$$

where the sum and the integration are extended to the bound and the continuum states, respectively, so that, accordingly, the index ν, in the last compact expression in Eq. (A4), represents either the integer index n or the continuum energy ϵ. $C_\nu(R')$ are linear combination coefficients. The functions $\varphi_\nu(R)$, spanning the whole vibrational bound-continuum spectrum of the resonant potential $V^-(R)$, are solutions of the equation

$$\left[-\frac{\hbar^2}{2M}\frac{d^2}{dR^2} + V^-(R) - E_\nu\right]\varphi_\nu(R) = 0, \quad \text{(A5)}$$

where E_ν are the vibrational eigenvalues.

To find the coefficients $C_\nu(R')$, expression (A4) must be inserted into Eq. (A2). Then, multiplying on the left by the operator $\int dR\varphi^*_{\nu'}(R)$, we get finally the linear system

$$\sum\!\!\!\!\!\!\int_\nu C_\nu(R')\left[(E_\nu - E)\delta_{\nu',\nu} - \frac{i}{2}\Gamma_{\nu'\nu}\right] = \varphi^*_{\nu'}(R'). \quad \text{(A6)}$$

Here Kronecker's $\delta_{\nu',\nu}$ should be replaced by the Dirac delta function $\delta(\nu-\nu')$ for values of ν and ν' both in the continuum. The matrix elements $\Gamma_{\nu',\nu}$ are defined as $\Gamma_{\nu',\nu} = \int dR\, \varphi^*_{\nu'}(R)\,\Gamma(R)\,\varphi_\nu(R)$.

In the case of the resonant Rydberg state $^2\Sigma_g^+$, the bound vibrational spectrum includes 13 wave functions only, while the continuum requires a large number of basis functions, which makes the solution of system (A6) for each R' value computationally expensive. In the present work we have used Eq. (A3) for the calculations of the cross sections discussed in the paper by solving Eq. (A2) using Numerov's method to get the solutions $u(R)$ and $v(R)$. System (A6) has been solved for the case $v = v' = 10$ only, by excluding the continuum spectrum, in order to obtain the approximated cross sections shown in Fig. 7 (dot-red curve).

Equation (A6) can be conveniently approximated. Let us rewrite the linear system as

$$C_{\nu'}(R')(E_{\nu'} - E) - \frac{i}{2}\sum\!\!\!\!\!\!\int_\nu C_\nu(R')\Gamma_{\nu'\nu} = \varphi^*_{\nu'}(R'). \quad \text{(A7)}$$

If we assume now that only the term $\nu = \nu'$ contributes to the sum we may write

$$C_{\nu'}(R') \approx \frac{\varphi^*_{\nu'}(R')}{E_{\nu'} - E - \frac{i}{2}\Gamma_{\nu'\nu'}}. \quad \text{(A8)}$$

This equation is rigorous when Γ is a constant since, in this case, in Eq. (A7) we can write $\Gamma_{\nu',\nu} = \Gamma\int dR\, \varphi^*_{\nu'}(R)\,\varphi_\nu(R)$.

However, we have verified numerically that Eq. (A8) provides a very good approximation for the combination coefficients, probably because $\Gamma_{\nu'\nu'}$ is not strongly dependent on ν' (see Table I). It shows also that the largest value for $C_{\nu'}$ is reached when $E_{\nu'=\bar{\nu}} = E$. Assuming that Green's function (A4) can be represented by this term only, we may write

$$G(R,R') \approx 2i \, \frac{\varphi^*_{\bar{\nu}}(R') \, \varphi_{\bar{\nu}}(R)}{\Gamma_{\bar{\nu}\bar{\nu}}}. \tag{A9}$$

This approximation is used in Eqs. (5) and (6) of the paper.

[1] M. Bacal, Nucl. Fusion **46**, S250 (2006); Chem. Phys. **398**, 3 (2012).
[2] U. Fantz, P. Franzen, and D. Wunderlich, Chem. Phys. **398**, 7 (2012).
[3] M. Baeva, W. J. Goedheer, and N. J. Lopes Cardozo, Plasma Sci. Technol. **10**, 162 (2008).
[4] U. Samm, in *Nuclear Fusion Research: Understanding Plasma-Surface Interactions*, edited by R. E. H. Clark and D. Reiter (Springer, Berlin, 2005).
[5] J. N. Bardsley and J. M. Wadehra, Phys. Rev. A **20**, 1398 (1979).
[6] J. Horáček, M. Čížek, K. Houfek, P. Kolorenč, and W. Domcke, Phys. Rev. A **70**, 052712 (2004).
[7] J. Horáček, M. Čížek, K. Houfek, P. Kolorenč, and W. Domcke, Phys. Rev. A **73**, 022701 (2006).
[8] G. J. Shultz, Phys. Rev. **113**, 816 (1959).
[9] H. Drexel, G. Senn, T. Fiegele, P. Scheier, A. Stamatovic, N. J. Mason, and T. D. Märk, J. Phys. B **34**, 1415 (2001).
[10] M. Allan, J. Phys. B **18**, L451 (1985).
[11] D. Rapp, T. E. Sharp, and D. D. Briglia, Phys. Rev. Lett. **14**, 533 (1965).
[12] E. Krishnakumar, S. Denifl, I. Čadež, S. Markelj, and N. J. Mason, Phys. Rev. Lett. **106**, 243201 (2011).
[13] J. Comer and F. H. Read, J. Phys. B **4**, 368 (1971).
[14] G. J. Shultz, Rev. Mod. Phys. **45**, 423 (1973).
[15] R. Celiberto, R. K. Janev, J. M. Wadehra, and A. Laricchiuta, Phys. Rev. A **77**, 012714 (2008).
[16] R. Celiberto, R. K. Janev, J. M. Wadehra, and A. Laricchiuta, Phys. Rev. A **80**, 012712 (2009).
[17] R. Celiberto, R. K. Janev, J. M. Wadehra, and J. Tennyson, Chem. Phys. **398**, 206 (2012).
[18] E. M. de Oliveira, M. A. P. Lima, and Márcio T. do N. Varella, Phys. Rev. A **78**, 042704 (2008).
[19] D. T. Stibbe and J. Tennyson, J. Phys. B **31**, 815 (1998).
[20] D. E. Atems and J. M. Wadehra, J. Phys. B **26**, L759 (1993).
[21] R. Celiberto, R. K. Janev, and D. Reiter, Plasma Phys. Control. Fusion **54**, 035012 (2012).
[22] D. T. Stibbe and J. Tennyson, Phys. Rev. Lett. **79**, 4116 (1997).
[23] C. Mündel, M. Berman, and W. Domcke, Phys. Rev. A **32**, 181 (1985).
[24] K. Houfek, M. Čížek, J. Horáček, Chem. Phys. **347**, 250 (2008).
[25] V. Laporta, R. Celiberto, and J. M. Wadehra, Plasma Sources Sci. Technol. **21**, 055018 (2012).
[26] V. Laporta, R. Celiberto, and J. Tennyson, Plasma Sources Sci. Technol. **22**, 025001 (2013).
[27] W. Kolos and L. Wolniewicz, J. Chem. Phys. **49**, 404 (1968).
[28] T. E. Sharp, Atomic Data **2**, 119 (1971).
[29] J. N. Bardsley and F. Mandl, Rep. Prog. Phys. **31**, 471 (1968).
[30] G. Arfken, *Mathematical Methods for Physicist*, 3rd ed. (Academic, New York, 1985).
[31] http://users.ba.cnr.it/imip/cscpal38/phys4entry/database.html.